Published OnlineFirst April 28, 2009; DOI: 10.1158/1940-6207.CAPR-08-0229

Objective Detection and Delineation of Oral Neoplasia Using Autofluorescence Imaging

Darren Roblyer,[1] Cristina Kurachi,[2] Vanda Stepanek,[3] Michelle D. Williams,[4] Adel K. El-Naggar,[4] J. Jack Lee,[5] Ann M. Gillenwater[3] and Rebecca Richards-Kortum[1]

Abstract Although the oral cavity is easily accessible to inspection, patients with oral cancer most often present at a late stage, leading to high morbidity and mortality. Autofluorescence imaging has emerged as a promising technology to aid clinicians in screening for oral neoplasia and as an aid to resection, but current approaches rely on subjective interpretation. We present a new method to objectively delineate neoplastic oral mucosa using autofluorescence imaging.

Autofluorescence images were obtained from 56 patients with oral lesions and 11 normal volunteers. From these images, 276 measurements from 159 unique regions of interest (ROI) sites corresponding to normal and confirmed neoplastic areas were identified. Data from ROIs in the first 46 subjects were used to develop a simple classification algorithm based on the ratio of red-to-green fluorescence; performance of this algorithm was then validated using data from the ROIs in the last 21 subjects. This algorithm was applied to patient images to create visual disease probability maps across the field of view. Histologic sections of resected tissue were used to validate the disease probability maps.

The best discrimination between neoplastic and nonneoplastic areas was obtained at 405 nm excitation; normal tissue could be discriminated from dysplasia and invasive cancer with a 95.9% sensitivity and 96.2% specificity in the training set, and with a 100% sensitivity and 91.4% specificity in the validation set. Disease probability maps qualitatively agreed with both clinical impression and histology. Autofluorescence imaging coupled with objective image analysis provided a sensitive and noninvasive tool for the detection of oral neoplasia.

Head and neck cancer, including cancers of the oral cavity, currently ranks as the sixth most common malignancy in the world. There were more than 270,000 new cases of oral cancer reported in 2002 (1). In the United States, approximately 50% of these individuals will present with stage III or IV disease, and 40% will die within 5 years of diagnosis (2). Screening individuals at risk for oral cancer and its precursors has the potential to improve early detection, providing the opportunity to intervene when treatment is most effective. In addition, surveillance of patients who have survived their initial oral cancer is important to identify local recurrences and second primary oral tumors, which occur at a higher rate than for any other tumor (3, 4).

Authors' Affiliations: [1]Department of Bioengineering, Rice University, Houston Texas; [2]São Carlos Institute of Physics, University of São Paulo, São Carlos, São Paulo, Brazil; and Departments of [3]Head and Neck Surgery, [4]Pathology, and [5]Biostatistics, University of Texas M. D. Anderson Cancer Center, Houston, Texas

Received 12/7/08; revised 1/16/09; accepted 2/6/09; published OnlineFirst 4/28/09.

Grant support: NIH grant nos. R21DE016485, R01CA095604, and P50CA097007.

Requests for reprints: Rebecca Richards-Kortum, Department of Bioengineering, Rice University, 6100 Main Street, Houston, TX 77251-1892. Phone: 713-348-3823; Fax: 713-348-5877; E-mail: RKortum@rice.edu.

doi:10.1158/1940-6207.CAPR-08-0229

Conventional oral examination using incandescent white light is the current standard of care for screening and surveillance for oral cancer and precancerous lesions. The sensitivity of visual examination is limited by several factors including the experience and index of suspicion of the examiners. In primary care situations, cases of malignancy may be rarely seen and clinicians may have difficulty discriminating the sometimes subtle mucosal changes associated with premalignant lesions and early cancers from more common benign inflammatory conditions (5). Furthermore, it can be challenging to delineate the boundaries of neoplastic lesions using conventional oral examination, making the choice of a biopsy location difficult.

Several new approaches have been proposed to address the limitations of conventional oral examination, including the use of toluidine blue, brush cytology, reflectance visualization after acetic acid application, and illumination with a chemiluminescent light source. Although useful in certain situations, each of these approaches is associated with a high rate of false-positives (5–8). Recently, several studies have shown that autofluorescence imaging may improve the ability to distinguish normal from premalignant and malignant oral tissue (9–15). When tissue is illuminated in the UV-visible region, a portion of photons are absorbed by molecules within the tissue called fluorophores which then emit lower energy photons

Published OnlineFirst April 28, 2009; DOI: 10.1158/1940-6207.CAPR-08-0229

that can be detected as fluorescence from the mucosal surface. Examples of fluorophores which produce autofluorescence signals in tissue include NADH and FAD in the epithelial layer, and collagen and elastin crosslinks in the stroma (16). In comparison with normal oral tissue, neoplastic lesions are associated with a decrease of green fluorescence when excited with UV or near-UV light (9, 10, 12, 17), which is attributed to decreased signal from collagen crosslinks in the stroma (18). Increased red fluorescence has also been observed by several groups in oral lesions and is frequently attributed to porphyrins (19). Several groups have proposed that this perceived loss of green fluorescence and increase in red fluorescence can be useful as a diagnostic aid to help detect and diagnose early neoplastic disease in several anatomic sites including the oral cavity, bronchus, cervix, esophagus, and colon (13, 20–23). In addition, the changes in fluorescence may aid in surgical resection by delineating the extent of neoplastic changes beyond the clinically apparent margins (9, 10).

Recently, the U.S. Food and Drug Administration approved an autofluorescence imaging device for early detection of oral neoplasia. The device, marketed as the VELscope (LED Dental, Inc., White Rock, British Columbia, Canada), uses a blue/violet light (400-460 nm wavelengths) to illuminate oral tissue and long-pass and notch filters to enable clinicians to directly visualize fluorescence in the oral cavity (9, 13). The VELscope and other proposed fluorescence imaging devices rely on qualitative observations to detect and delineate neoplastic oral lesions and therefore reliable screening with these instruments necessitates well-defined and standardized image interpretation criteria, and appropriate user training. This may not be feasible in many primary care situations. We hypothesize that the application of digital image processing techniques to autofluorescence imaging of oral tissue will provide the ability to objectively identify and delineate the peripheral extent of neoplastic lesions in the oral cavity. This will provide a powerful tool in patient care locations where experts are not available or where physicians encounter few cases of malignant and premalignant neoplasia. Low-cost digital cameras with sufficient sensitivity to record tissue autofluorescence in near real-time are now readily available (24), making the clinical application of such automated image processing feasible.

The primary goal of the present study was to evaluate the use of quantitative autofluorescence imaging for the detection and delineation of oral neoplastic lesions. We show that a simple, objective method can be used to accurately classify regions of interest (ROI) within an autofluorescence image with 100% sensitivity and 91.4% specificity relative to histopathology. This method can delineate the presence and extent of neoplastic lesions within a field of view and provide results which correlate with the histopathologic assessment of extent of disease. Thus, quantitative autofluorescence imaging may provide a noninvasive and objective method to improve screening and margin delineation of oral cancers and precancers.

Materials and Methods

Human subjects

Study subjects were enrolled in a clinical protocol reviewed and approved by the Institutional Review Boards at The University of Texas M.D. Anderson Cancer Center and Rice University. Patients were eligible and recruited if they were 18 years of age or older, and had known or suspected precancerous or cancerous squamous lesions located in the oral mucosa. Patients may have had previous surgical, radiation, or chemotherapeutic treatments. Normal volunteers were eligible and recruited if they were 18 years of age or older and had no history of oral pathology. All subjects enrolled in the study gave written informed consent. The average age of patients in this study was 59, 42% of the patients were female and 58% were male. The average age of normal volunteers in this study was 27.4, 27% were female and 73% were male.

Imaging procedure

Autofluorescence images were obtained from the oral cavity of 56 patients with clinically abnormal lesions and 11 normal volunteers. Data were divided into a training set and a validation set. Data acquired from the first 39 patients and 7 normal volunteers imaged between June 2006 and January 2008 were allocated to the training set, and were used to develop an algorithm for the detection of neoplasia. Data acquired from the subsequent 17 patients and 4 normal volunteers imaged between March and June 2008 formed a validation set and were used to test the performance of this algorithm relative to histopathology.

White light and autofluorescence images were obtained at 365, 380, 405, and 450 nm excitation using a Multispectral Digital Microscope. This device is described in detail elsewhere (25), but briefly, the Multispectral Digital Microscope is a wide-field optical microscope which collects digital autofluorescence and reflectance images with a color CCD camera from a variable field of view, ranging in size from ~1 to 7 cm. Patients were imaged either in an outpatient clinic or in the operating room under general anesthesia prior to surgery. A physician positioned the patient and microscope so that the suspicious lesion or area of interest was clearly in the field of view of the device. Clinically normal areas distant from or contralateral to the lesion were also imaged. Following imaging in the clinic, suspicious lesions were biopsied. In the operating room, previously biopsied lesions were surgically resected.

Histopathologic correlation

Biopsies and resected tissues were evaluated using standard histopathologic analysis by a board-certified pathologist (either A. El-Naggar or M.D. Williams). The location of biopsies and resected lesions was recorded using digital photography so that pathology results could later be correlated to multispectral imaging results. In addition, the locations of gross anatomic features were noted in both autofluorescence images and histology specimens to aid in correlation. The resulting histopathology sections were evaluated to provide a diagnosis along the entire length of the epithelium, also noting any submucosal abnormalities in each slide. Histopathology diagnosis included the following categories: normal, mild dysplasia, moderate dysplasia, severe dysplasia/carcinoma *in situ*, and invasive carcinoma. For the purposes of diagnostic algorithm development, two major categories were defined: normal tissue (including inflammation and hyperplasia) and neoplastic tissue (including dysplasia, carcinoma *in situ*, and cancer).

Analysis and statistical methods

Images were preprocessed to subtract signals from ambient room light and translated so that white light and fluorescence images of the same field of view were spatially registered. Two hundred and seventy-six measurements corresponding to 159 unique ROI sites of clinically normal and suspicious regions of tissue were selected from white light images by a head and neck surgeon (A.M. Gillenwater) blinded to the results of the autofluorescence imaging. In some cases, repeat measurements were obtained from the same ROI site to help ensure image data was collected without motion artifacts; often both the first and repeat measurements were included in the analysis. These repeat measurements account for the difference between the number of measurements and the number of ROI sites. Heterogeneity in pathologic diagnoses may occur within relatively small areas of

Published OnlineFirst April 28, 2009; DOI: 10.1158/1940-6207.CAPR-08-0229

diseased oral mucosa (26, 27), therefore, ROIs were stringently selected from suspicious areas using one of the following four criteria: (*a*) areas corresponding to the same size and location as a biopsy with a pathologic diagnosis, (*b*) ROIs from locations which could be correlated to a histopathology slide with a corresponding pathologic diagnosis, (*c*) areas within well-defined exophytic tumors confirmed by pathologic diagnosis, and (*d*) ROIs from a location which was clinically normal and deemed by the physician to be sufficiently distant from the lesion.

Autofluorescence images from the training set were analyzed to determine whether specific image features could be used to classify a measurement site as normal or neoplastic. The autofluorescence images and white light images were spatially registered so that the ROIs chosen in the white light images corresponded to the same region of tissue in the autofluorescence images. The training set included data from the first 39 patients and 7 normal volunteers and included measurements from 173 measurements of 102 unique ROIs. Qualitatively, neoplastic ROIs were associated with a decrease in average green fluorescence intensity and often an increase in red fluorescence intensity. The mean ratio of red-to-green pixel intensities inside each of the ROIs was calculated from the fluorescence images at each excitation wavelength. Red and green pixel intensities were obtained from the collected Red-Green-Blue color images, created by the Bayer color mask on the CCD detector. A classifier was developed to distinguish neoplastic and normal ROIs using linear discriminant analysis with the single input feature of average ratio of red-to-green fluorescence. When more than one measurement corresponded to a ROI site, the mean of the feature values was used for classification. The classifier was trained using all of the ROI sites in the training set and the prior probability input into the classifier was chosen to represent the percentage of abnormal to normal measurements in the data set. The classifier was developed after images were acquired from patients in the training set but before measurements were acquired from patients in the validation set. Classifier accuracy in the training set was assessed by plotting the receiver operating characteristic (ROC) curve, the area under the ROC curve (AUC), and the sensitivity and specificity at a particular operating point on the ROC curve (28–30). The positive and negative predictive values were also calculated at the operating point. Confidence intervals (CI) were calculated for operating characteristics using the Wilson "score" method including a continuity correction (31).

The algorithm was then applied to data from the validation set using the red-to-green ratio threshold found to produce the highest combination of sensitivity and specificity in the training set. The validation set was designed to rigorously test the algorithm, and for most patients, ROI and biopsy pairs were collected on the clinical margins of the lesion in addition to directly on the lesion and in clinically normal areas. The validation set included 103 measurements from 57 unique ROIs in a second group of 17 patients and 4 normal volunteers.

An additional analysis step was explored to increase the performance of the classifier by normalizing the red-to-green ratio measurements for each patient. An additional unique and nonoverlapping ROI of clinically normal tissue was chosen from the same anatomic site and in the same field of view for each of the ROIs described above. At each excitation wavelength, the mean red-to-green autofluorescence ratio was calculated in this ROI; the mean red-to-green ratios from the other ROIs were normalized by this value. This method provides a way to compensate for anatomic and patient to patient variations in red-to-green fluorescence intensity ratio. Identical statistical analysis was done using this measured feature with both the training set and the validation set. The method using the magnitude of the red-to-green fluorescence intensity ratio is termed the raw red-to-green method and the method using a normalized red-to-green fluorescence intensity ratio is termed normalized red-to-green method.

Disease probability maps

The classification algorithms described above provided a relationship between the magnitude of the red-to-green fluorescence intensity ratio for a particular region of interest within the image and the probability of that region having a diagnosis of abnormal. This relationship was used to predict the probability of a diagnosis of dysplasia or cancer for each pixel in an image, given the normalized red-to-green fluorescence intensity ratio at that pixel. The posterior probability values at each pixel in the image were computed and pixels which corresponded to a 50% or greater probability of being classified as dysplastic or cancerous were color-coded and digitally overlaid onto the white light images. This method provides a means to illustrate areas of tissue with the highest probability of being neoplastic. The assumption was made that the region of interest method described above could be generalized on a pixel by pixel basis. Disease probability maps were compared with histologic images of tissue resected from the field of view to confirm the accuracy of this method.

Results

Tables 1 and 2 summarize the anatomic site and histopathologic diagnoses of the 159 sites included in this analysis. The most common sites were the tongue, buccal mucosa, and floor of the mouth, followed by the palate, lip, and gingiva. The training set contained 52% normal, 28% dysplastic, and 20% invasive carcinoma sites, whereas the validation set contained 61% normal, 25% dysplastic, and 14% invasive carcinoma sites. The normal histopathologic category could include tissue with hyperkeratosis, hyperplasia, and/or inflammation as long as there was no dysplasia or carcinoma. The normal sites in the training set, based on available pathology (not including normal volunteers and normal sites in which no biopsy was taken), included seven sites (13.2% of normal sites) with hyperplasia and hyperkeratosis, four sites (7.5% of normal sites) with hyperkeratosis, and three sites (5.7% of normal sites) with hyperplasia and/or fibroadipose tissue. The validation set included three sites (8.6% of normal sites) with hyperplasia and hyperkeratosis, one site (2.9% of normal sites) with hyperplasia, one site (2.9% of normal sites) with a submucosal hemorrhage, and one site (2.9% of normal sites) with marked inflammation and osteonecrosis. The abnormal histopathology category could include dysplasia and carcinoma. In the training set, 59.2% of the abnormal sites were premalignant (mild, moderate, or severe dysplasia); in the validation set, 63.6% of the abnormal sites were premalignant.

Figure 1 shows white light and autofluorescence images from the buccal mucosa of a patient with pathologically

Table 1. Anatomic sites of ROIs in the training and validation set

Anatomic site	No. of sites in the training set (%)	No. of sites in the validation set (%)
Tongue	37 (36.3)	19 (33.3)
Buccal mucosa	12 (11.8)	15 (26.3)
Floor of mouth	22 (21.6)	4 (7.0)
Gingiva	2 (2.0)	7 (12.3)
Lip	14 (13.7)	4 (7.0)
Palate	15 (14.7)	8 (14.0)
Total	102 (100)	57 (100)

NOTE: Percentages may not add up to 100% because of rounding.

Published OnlineFirst April 28, 2009; DOI: 10.1158/1940-6207.CAPR-08-0229

Table 2. Pathology diagnosis of ROI sites in the training and validation sets

Diagnosis	No. of sites in the training set (%)	No. of sites in the validation set (%)
Normal	53 (52.0)	35 (61.4)
Mild dysplasia	11 (10.8)	5 (8.8)
Moderate dysplasia	6 (5.9)	5 (8.8)
Severe dysplasia/CIS	12 (11.8)	4 (7.0)
Invasive carcinoma	20 (19.6)	8 (14.0)
Total	102 (100)	57 (100)

confirmed invasive carcinoma. The white light image (Fig. 1A) shows two ROIs, one of which corresponds to a pathologically confirmed invasive carcinoma, and the other which was clinically normal and outside of the pathologically confirmed clear resection margin. Figure 1B-D show autofluorescence images at different excitation wavelengths that were taken before surgery from the same field of view. The autofluorescence image obtained at 405 nm excitation qualitatively shows the greatest visual contrast between the normal and neoplastic ROI. This observation was typical for study patients.

Table 3 summarizes the performance of both diagnostic algorithms, based on either the raw or the normalized mean red-to-green fluorescence intensity ratios, for classifying lesions in the training set. At each excitation wavelength, the classifier that used the normalized red-to-green fluorescence intensity ratio (normalized R/G ratio) had slightly higher AUC than the algorithm based on the raw red-to-green fluorescence intensity ratio (raw R/G ratio). In all cases, the highest AUC was obtained at 405 nm excitation. The sensitivity and specificity values at the point on the ROC curve nearest the gold standard (Q-point) are also reported in Table 3.

A scatter plot of the normalized red-to-green ratio at 405 nm excitation for each of the 102 sites in the training set, as well as the threshold of 1.19 used in the classification algorithm, is shown in Fig. 2A. Of the 102 sites, 4 were misclassified, including 1 site of fibroadipose tissue on the lower lip misclassified as abnormal, 1 hyperkeratotic site on the right buccal misclassified as abnormal, 1 cancer site on the right lateral tongue misclassified as normal, and 1 site on the left soft palate with focal ulceration and dysplasia misclassified as normal. Figure 2B shows the ROC curve for this classifier; the AUC is 0.988, and at the Q-point, the sensitivity was 95.9% (95% CI, 84.9-99.3%) and the specificity was 96.2% (95% CI, 85.9-99.3%). The positive predictive value was 95.9% (95% CI, 84.9-99.3%) and the negative predictive value was 96.2% (95% CI, 85.9-99.3%). This operating point is indicated on the ROC curve.

The algorithm using the normalized red-to-green fluorescence intensity ratio at 405 nm excitation was applied to the validation set. In Fig. 2C, a scatter plot of the normalized R/G ratio for each site in the validation set is shown along with the threshold that had been previously selected for the training set. Figure 2D depicts the ROC curve with the operating point selected for the training set indicated. A 100% sensitivity (95% CI, 81.5-100%) and 91.4% specificity (95% CI, 75.8-97.8%) and an AUC of 0.987 were achieved at this operating point for the validation set. The positive predictive value was 88.0% (95% CI, 67.7-96.9%) and the negative predictive value was 100% (95% CI, 86.7-100%). Of the 57 sites in the validation set, 3 were misclassified as abnormal including 1 site on the left buccal with hyperplasia, 1 site on the right buccal, and another site on the left buccal.

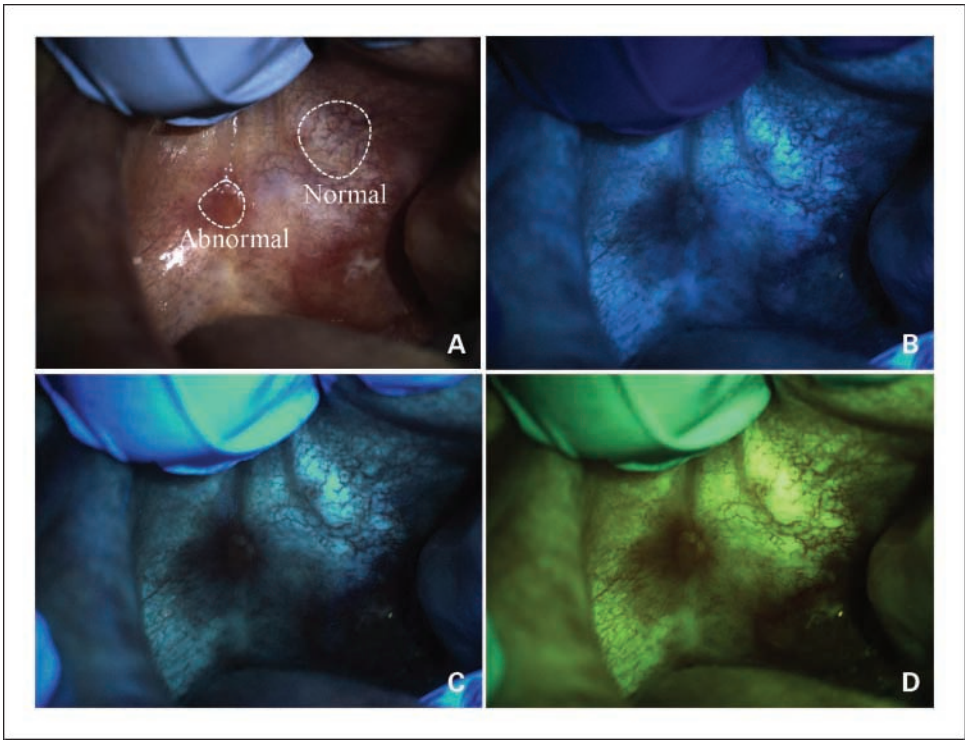

Fig. 1. Autofluorescence and white light images of the buccal mucosa of a typical study patient. *A*, white light image showing regions of interest of histopathologically confirmed normal tissue and invasive carcinoma. *B*, fluorescence image at 365 nm excitation. *C*, fluorescence image at 405 nm excitation. *D*, fluorescence image at 450 nm excitation.

Published OnlineFirst April 28, 2009; DOI: 10.1158/1940-6207.CAPR-08-0229

Table 3. Classification results at each fluorescence excitation wavelength using both the raw R/G ratio method and the normalized R/G ratio method in the training set

Fluorescence excitation wavelength (nm)	Raw R/G ratio			Normalized R/G ratio		
	AUC	Sensitivity (%)	Specificity (%)	AUC	Sensitivity (%)	Specificity (%)
365	0.832	83.7	73.6	0.856	83.7	86.8
380	0.891	89.8	77.4	0.924	83.7	88.7
405	0.971	91.8	92.5	0.988	95.9	96.2
450	0.922	81.6	92.5	0.906	85.7	90.6

Figure 3 shows white light– and 405 nm–excited autofluorescence images from a study patient with moderate dysplasia and carcinoma *in situ* located on the floor of mouth. The white light image is also shown with an overlay of the calculated disease probability map; regions corresponding to a predictive probability of a neoplastic lesion greater than 50% are shaded as indicated by the color bar. The disease probability map indicates the probability that a particular pixel in the image corresponds to a neoplastic area of tissue. Histologic sections obtained at six areas in the tissue are also shown. Only one of these areas was included in the previous classification analysis. The disease probability map shows qualitative agreement with the presence of dysplasia and cancer in the areas corresponding to the histologic sections.

Figure 4 shows representative white light images with and without superimposed disease probability maps from four study patients. Images in the first three rows correspond to patients with histologically confirmed neoplasia, whereas the image in the bottom row is from a normal volunteer with no clinically suspicious lesions. Although the lesion in Fig. 4A is obvious, those in B and C are less so, highlighting the potential to aid clinicians in identifying the presence of neoplasia and identifying optimal sites for further evaluation with biopsy. Images in Fig. 4A and B are from a patient with an invasive carcinoma on the floor of mouth. Images in Fig. 4C and D are from a patient with a region of severe dysplasia on the tongue. The images in Fig. 4E and F are from a patient with a region of moderate dysplasia on the gingiva. In all three cases, the disease probability map delineates the suspicious regions identified clinically by an oral cancer specialist blinded to the results of the autofluorescence imaging and are consistent with histopathologic

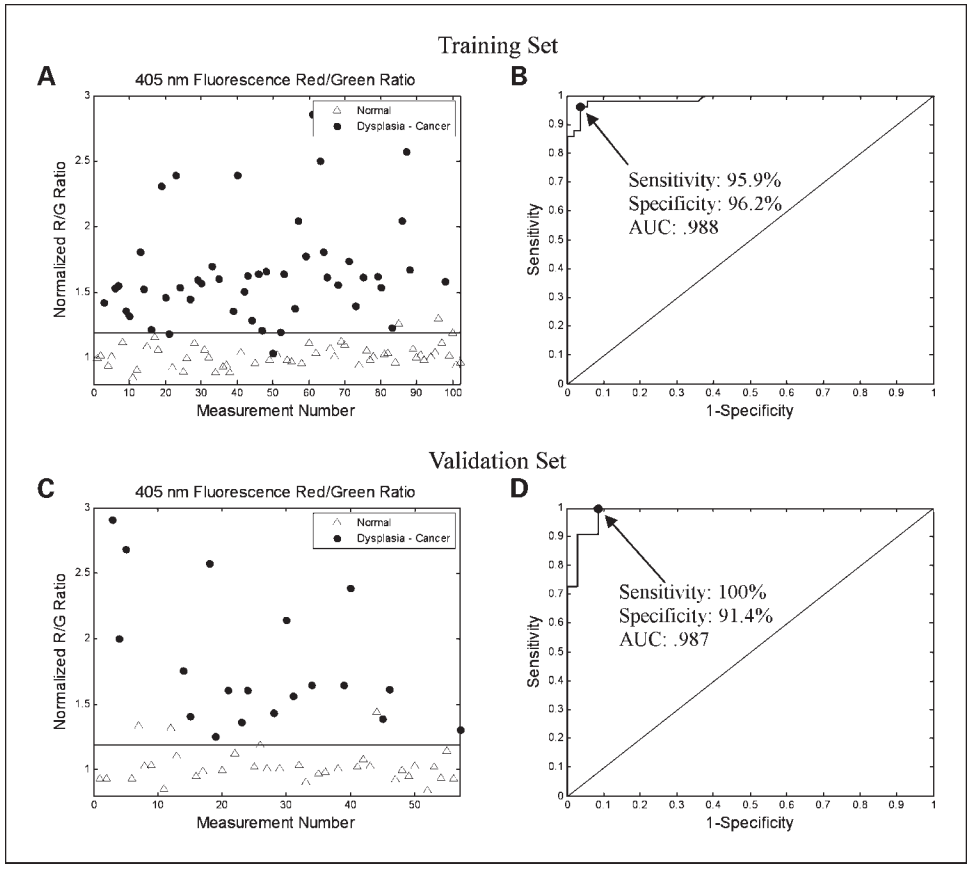

Fig. 2. *A,* scatter plot of normalized red-to-green ratios at 405 nm excitation for the 102 ROI sites in the training set. Horizontal line, the threshold used to obtain 95.9% sensitivity and 96.2% specificity. Note that two additional abnormal data points had a red-to-green fluorescence intensity ratio >3 but are not shown on this plot. *B,* ROC curve of the classifier based on the normalized red-to-green ratio. Dot and arrow, the operating point used for classification. *C,* scatter plot of the red-to-green ratio for the 57 sites in the validation set with threshold selected from the training set indicated. Note that three additional abnormal data points had a red-to-green fluorescence intensity ratio >3 but are not shown on this plot. *D,* ROC curve obtained for the validation set. The operating point is indicated and corresponds to the threshold chosen from the training set.

Published OnlineFirst April 28, 2009; DOI: 10.1158/1940-6207.CAPR-08-0229

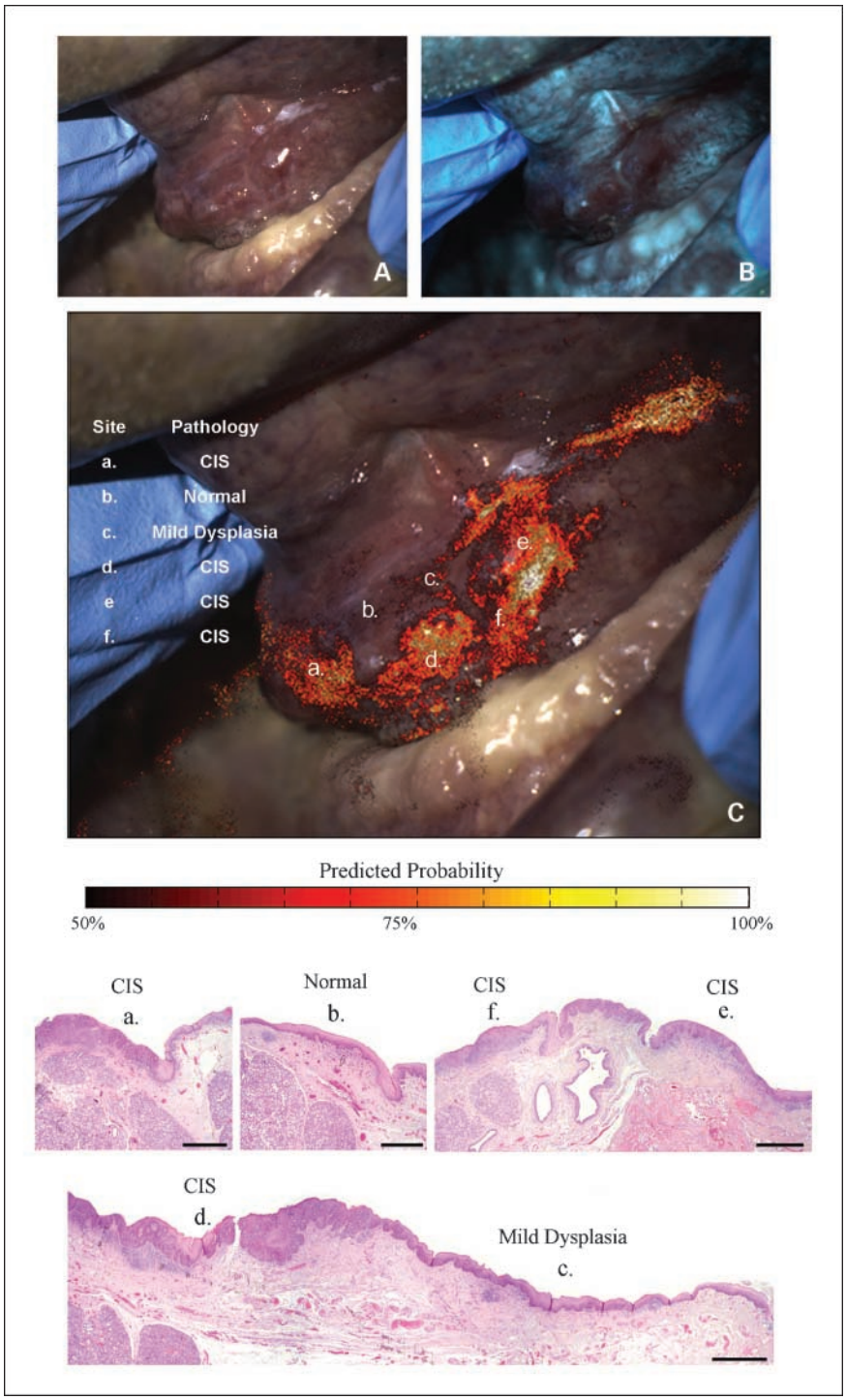

Fig. 3. *A,* white light image of floor of the mouth with histopathologically confirmed dysplasia and carcinoma *in situ. B,* 405 nm excitation fluorescence image showing areas with deceased autofluorescence. *C,* white light image with disease probability map showing the predictive probability of a neoplastic lesion superimposed. Letters indicate specific locations where pathology is known. The key indicates pathology. The histology slides show tissue sections from these areas (*bottom*). Bar, 1 mm.

sections obtained. Figure 4G and H are from the inner lip of a normal volunteer and the disease probability map does not indicate any lesions.

Discussion

Our results illustrate how autofluorescence imaging may enhance the ability of clinicians to detect and delineate areas of oral dysplasia and carcinoma. Although all four illumination conditions tested allowed the visualization of changes in autofluorescence with neoplasia, illumination with the 405 nm wavelength produced the highest discriminatory capability. This corresponds to previous findings comparing illumination wavelengths for autofluorescence imaging in freshly resected oral cancer surgical specimens (17). Although subjective interpretation of loss of autofluorescence has been shown to be useful (9, 13), there are several important advantages associated with objective and quantitative analysis of changes in autofluorescence signal. First, quantitative analysis methods provide a rigorous and repeatable way to determine the

Published OnlineFirst April 28, 2009; DOI: 10.1158/1940-6207.CAPR-08-0229

threshold for demarcating a lesion, even for providers with less experience. Second, digital imaging allows the operator to save and process images, directly comparing data from multiple patients in a series or from a single patient over time. Third, ratios of fluorescence intensity values provide a way to reduce variations in images associated with spatial nonuniformities in illumination.

In the present study, the performance of a simple classifier based on the ratio of red-to-green autofluorescence intensity at 405 nm excitation was tested and found to discriminate

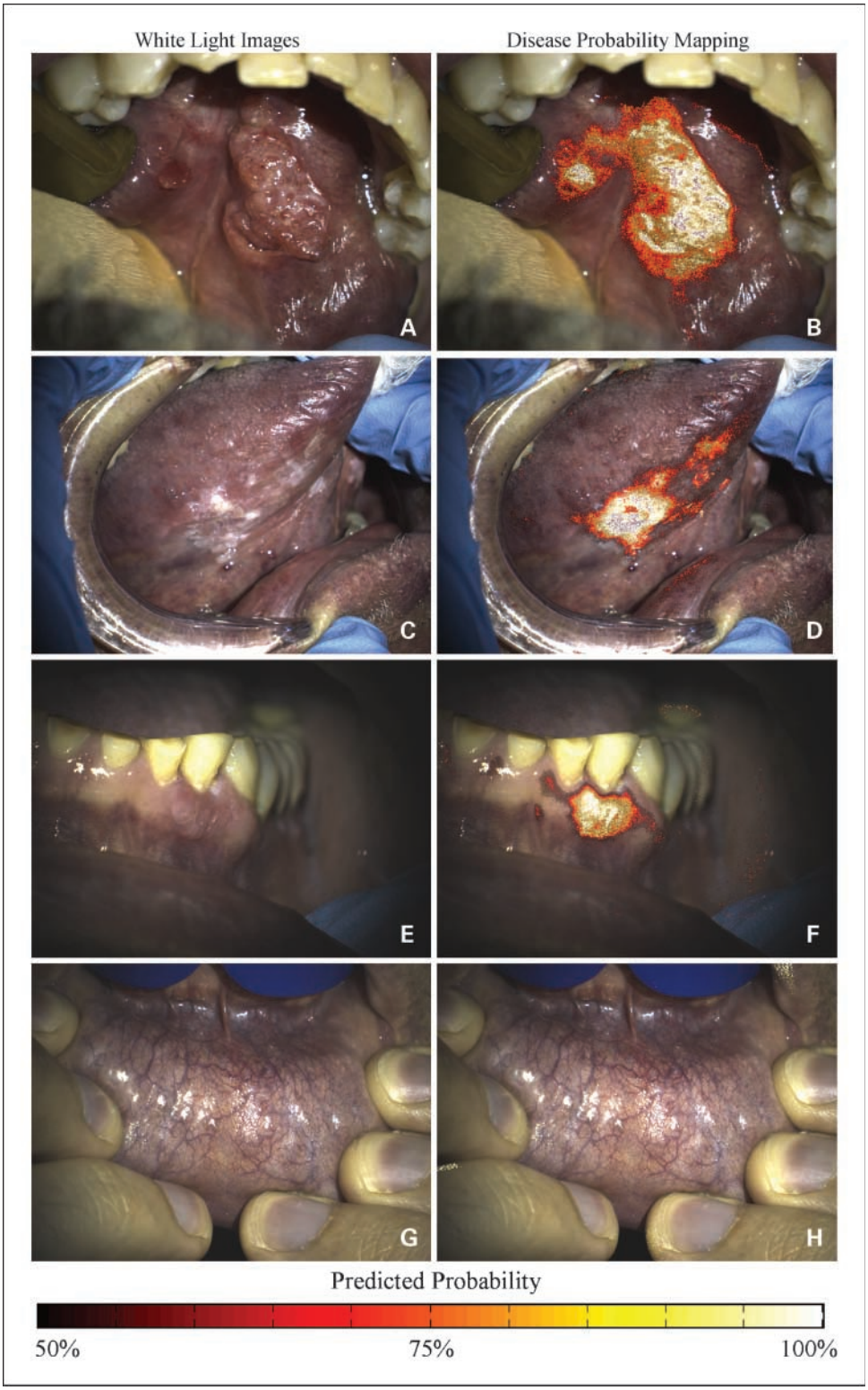

Fig. 4. *A* and *B*, images from a patient with an invasive carcinoma on the floor of the mouth. *A*, white light image; *B*, white light image with disease probability mapping showing the predictive probability of a neoplastic lesion; *C* and *D*, images from a patient with a region of severe dysplasia on the tongue; *E* and *F*, images from a patient with a region of moderate dysplasia on the gingiva; *G* and *H*, images from the inner lip of a normal volunteer.

Published OnlineFirst April 28, 2009; DOI: 10.1158/1940-6207.CAPR-08-0229

neoplastic and nonneoplastic tissue with a sensitivity and specificity of 96% in the training set and 100% sensitivity and 91.4% specificity in the validation set. These results compare favorably with the performance of visual oral examination, which has been systematically reviewed by Downer et al. (32). Downer identified eight prospective studies between 1980 and 2002 that involved conventional oral exam with gold standard verification provided by an expert observer. In four of the studies, the screeners were general dentists and in four of the studies, the screeners were trained health workers. Sensitivity ranged from 59% to 97%, specificity ranged from 75% to 99%, and meta-analysis resulted in a weighted pooled sensitivity of 85% and a specificity of 97%. Other reports of the performance of visual oral screening include Sankaranarayanan et al. (sensitivity 77%, specificity 76%; ref. 33), Ramadas et al. (sensitivity 82%, specificity 85%; ref. 34), and Nagao et al. (sensitivity 92%, specificity 64%; ref. 35). The classifier in this study can be applied to entire images of the oral cavity to visualize areas with a high probability of being neoplastic; disease probability maps are consistent with histologic sections obtained from tissue in the field of view.

Autofluorescence imaging has shown great promise for enhancing the visualization of neoplastic areas in recent studies (9, 10, 13–15, 17). In a study of 44 patients, Lane et al. showed high sensitivity and specificity in discriminating normal oral mucosa from severe dysplasia, carcinoma *in situ*, or invasive carcinoma based on visual assessment of loss of autofluorescence in diseased mucosa at excitation wavelengths between 400 and 460 nm (13). In another study by the same group, the potential for autofluorescence imaging to enhance delineation of the margins of neoplastic changes was shown. In some cases, fluorescence loss extended as far as 25 mm beyond the clinically apparent margin (9). Autofluorescence endoscopic imaging technologies for lung and the gastrointestinal tract using ratios of red and green signal have been available for over a decade and have greatly increased the sensitivity of disease detection in these organ systems (20, 36–38). The laser-induced fluorescence emission (LIFE) system is an autofluorescence bronchoscopy device which provides the user with a real-time image in which changes in hue correspond to suspicious and/or abnormal areas. Users of the device must be trained in order to interpret these changes in image hue (37).

A potential confounding factor which may limit the specificity of classifiers based on the red-to-green fluorescence intensity ratio for automated image analysis software is the frequent presence of red fluorescence on normal papillae of the dorsal aspect of the tongue. At 405 nm excitation, increased fluorescence above 600 nm emission has been observed in oral lesions and is thought to originate from porphyrins, although it is uncertain whether the origins of these porphyrins are intrinsic or derived from bacterial contamination (39). Red porphyrin-like fluorescence has been shown to correlate with neoplastic disease in other regions of the oral cavity (10, 39). However, normal red fluorescence is limited to the dorsal tongue; it is not observed on normal areas on the lateral and ventral tongue where there is a much higher propensity for developing neoplastic disease (40). In this study, a single site in the training set was imaged on the dorsal tongue and corresponded to cancer. Bright red fluorescence was visible at this site.

Our results show the potential of quantitative fluorescence imaging as an objective approach to noninvasively identify and delineate the mucosal extent of neoplastic lesions in the oral cavity. It should be noted that the images were obtained with a research-grade device and the disease probability maps described here were constructed subsequent to the image acquisition and compared with only a limited number of sites with diagnosis confirmed using histopathology. Unfortunately, it is difficult to obtain pathology diagnosis for the entire surface of a resected specimen. Additionally, in order to provide optimal benefit to clinicians both for detection and margin delineation of oral dysplasia and carcinoma, these disease probability maps need to be available to view in real or near real-time. We are currently making software improvements and developing quantitative fluorescence imaging devices that can show false color disease probability maps based on red-to-green fluorescence intensity ratios at 405 nm excitation at the time of the examination. In addition, we recognize that our results were obtained from a small group of subjects with disease prevalence that might be expected in a treatment population rather than a screening population. Future studies are planned to evaluate this method of quantitative fluorescence imaging in community settings in a larger subject group with a wide spectrum of oral pathologies including oral dysplasia and early invasive disease, benign conditions, and inflammation.

In summary, the present study provides proof-of-principle for the use of a practical tool for quantitative fluorescence imaging as an objective technique for detection and delineation of oral neoplasia. The use of objective disease probability maps represents an important advance towards the integration of optical imaging technologies into the clinical practice of dentists and primary health care workers. The development of noninvasive and objective diagnostic aids based on these findings may facilitate the early detection and diagnosis of oral cancer and its precursors by less experienced personnel at the point of care.

Disclosure of Potential Conflicts of Interest

Dr. Richards-Kortum serves as an unpaid scientific advisor to Remicalm LLC, holds patents related to optical diagnostic technologies that have been licensed to Remicalm LLC, and holds minority ownership in Remicalm LLC. Dr. Gillenwater has served as a paid consultant to Sanofi-Adventis, U.S. LLC, has a minority equity interest in Onconome, Inc., and serves as an unpaid scientific advisor to Remicalm LLC.

References

1. Parkin DM, Bray F, Ferlay J, Pisani P. Global cancer statistics, 2002. CA Cancer J Clin 2005; 55:74–108.
2. Ries LAG, Young JL, Keel GE, Eisner MP, Lin YD, Horner M-J (editors). SEER Survival Monograph: Cancer Survival Among Adults: U.S. SEER Program, 1988–2001, Patient and Tumor Characteristics. National Cancer Institute, SEER Program, NIH Pub. No. 07-6215, Bethesda, MD, 2007.
3. Lippman SM, Hong WK. Second malignant tumors in head and neck squamous cell carcinoma: the overshadowing threat for patients with early-stage disease. Int J Radiat Oncol Biol Phys 1989;17:691–4.
4. Day GL, Blot WJ. Second primary tumors in patients with oral cancer. Cancer 1992;70:14–9.
5. Lingen MW, Kalmar JR, Karrison T, Speight PM. Critical evaluation of diagnostic aids for the detection of oral cancer. Oral Oncol 2008;44:10–22.
6. Gillenwater A, Papadimitrakopoulou V, Richards-Kortum R. Oral premalignancy: new methods of

Published OnlineFirst April 28, 2009; DOI: 10.1158/1940-6207.CAPR-08-0229

detection and treatment. Curr Oncol Rep 2006;8:146–54.

7. Oh ES, Laskin DM. Efficacy of the ViziLite system in the identification of oral lesions. J Oral Maxillofac Surg 2007;65:424–6.

8. Rosin MP, Poh CF, Guillard M, Williams PM, Zhang L, MacaUlay C. Visualization and other emerging technologies as change makers for oral cancer prevention. Ann N Y Acad Sci 2007;1098:167–83.

9. Poh CF, Zhang L, Anderson DW, et al. Fluorescence visualization detection of field alterations in tumor margins of oral cancer patients. Clin Cancer Res 2006;12:6716–22.

10. De Veld DC, Witjes MJ, Sterenborg HJ, Roodenburg JL. The status of *in vivo* autofluorescence spectroscopy and imaging for oral oncology. Oral Oncol 2005;41:117–31.

11. Svistun E, Alizadeh-Naderi R, El-Naggar A, Jacob R, Gillenwater A, Richards-Kortum R. Vision enhancement system for detection of oral cavity neoplasia based on autofluorescence. Head Neck 2004;26:205–15.

12. Utzinger U, Bueeler M, Oh S, et al. Optimal visual perception and detection of oral cavity neoplasia. IEEE Trans Biomed Eng 2003;50:396–9.

13. Lane PM, Gilhuly T, Whitehead P, et al. Simple device for the direct visualization of oral-cavity tissue fluorescence. J Biomed Opt 2006;11:024006.

14. Kulapaditharom B, Boonkitticharoen V. Laser-induced fluorescence imaging in localization of head and neck cancers. Ann Otol Rhinol Laryngol 1998;107:241–6.

15. Andersson-Engels S, Klinteberg C, Svanberg K, Svanberg S. *In vivo* fluorescence imaging for tissue diagnostics. Phys Med Biol 1997;42:815–24.

16. Richards-Kortum R, Sevick-Muraca E. Quantitative optical spectroscopy for tissue diagnosis. Annu Rev Phys Chem 1996;47:555–606.

17. Svistun E, Alizadeh-Naderi R, El-Naggar A, Jacob R, Gillenwater A, Richards-Kortum R. Vision enhancement system for detection of oral cavity neoplasia based on autofluorescence. Head Neck 2004;26:205–15.

18. Pavlova I, Williams M, El-Naggar A, Richards-Kortum R, Gillenwater A. Understanding the biological basis of autofluorescence imaging for oral cancer detection: high-resolution fluorescence microscopy in viable tissue. Clin Cancer Res 2008;14:2396–404.

19. de Veld DC, Skurichina M, Witjes MJ, Duin RP, Sterenborg HJ, Roodenburg JL. Clinical study for classification of benign, dysplastic, and malignant oral lesions using autofluorescence spectroscopy. J Biomed Opt 2004;9:940–50.

20. Lam S, MacAulay C, Palcic B. Detection and localization of early lung cancer by imaging techniques. Chest 1993;103:12–4S.

21. Park SY, Follen M, Milbourne A, et al. Automated image analysis of digital colposcopy for the detection of cervical neoplasia. J Biomed Opt 2008;13:014029.

22. Kara MA, Peters FP, Fockens P, ten Kate FJ, Bergman JJ. Endoscopic video-autofluorescence imaging followed by narrow band imaging for detecting early neoplasia in Barrett's esophagus. Gastrointest Endosc 2006;64:176–85.

23. Matsuda T, Saito Y, Fu KI, et al. Does autofluorescence imaging videoendoscopy system improve the colonoscopic polyp detection rate? A pilot study. Am J Gastroenterol 2008;103:1926–32.

24. Rahman M, Chaturvedi P, Gillenwater A, Richards-Kortum R. Low-cost, multimodal, portable screening system for early detection of oral cancer. J Biomed Opt 2008;13:030502.

25. Roblyer D, Richards-Kortum R, Sokolov K, et al. Multispectral optical imaging device for *in vivo* detection of oral neoplasia. J Biomed Opt 2008;13:024019.

26. Slaughter DP, Southwick HW, Smejkal W. Field cancerization in oral stratified squamous epithelium; clinical implications of multicentric origin. Cancer 1953;6:963–8.

27. Braakhuis BJ, Tabor MP, Kummer JA, Leemans CR, Brakenhoff RH. A genetic explanation of Slaughter's concept of field cancerization: evidence and clinical implications. Cancer Res 2003;63:1727–30.

28. Duda RO, Hart PE, Stork DG. Pattern classification. 2nd ed New York: John Wiley & Sons, Inc.; 2001.

29. Zhou X-H, McClish DK, Obuchowski NA. Statistical methods in diagnostic medicine. New York: John Wiley & Sons; 2002.

30. Albert A, Harris EK. Multivariate interpretation of clinical laboratory data. New York: Marcel Dekker, Inc.; 1987.

31. Newcombe RG. Two-sided confidence intervals for the single proportion: comparison of seven methods. Stat Med 1998;17:857–72.

32. Downer MC, Moles DR, Palmer S, Speight PM. A systematic review of test performance in screening for oral cancer and precancer. Oral Oncol 2004;40:264–73.

33. Sankaranarayanan R, Mathew B, Jacob BJ, et al. Early findings from a community-based, cluster-randomized, controlled oral cancer screening trial in Kerala, India. The Trivandrum Oral Cancer Screening Study Group. Cancer 2000;88:664–73.

34. Ramadas K, Sankaranarayanan R, Jacob BJ, et al. Interim results from a cluster randomized controlled oral cancer screening trial in Kerala, India. Oral Oncol 2003;39:580–8.

35. Nagao T, Ikeda N, Fukano H, Miyazaki H, Yano M, Warnakulasuriya S. Outcome following a population screening programme for oral cancer and precancer in Japan. Oral Oncol 2000;36:340–6.

36. Zeng H, MacAulay C. Real-time endoscopic fluorescence imaging for early cancer detection in the gastrointestinal tract. Bioimaging 1998;6:151–65.

37. Kurie JM, Lee JS, Morice RC, et al. Autofluorescence bronchoscopy in the detection of squamous metaplasia and dysplasia in current and former smokers. J Natl Cancer Inst 1998;90:991–5.

38. Hirsch FR, Prindiville SA, Miller YE, et al. Fluorescence versus white-light bronchoscopy for detection of preneoplastic lesions: a randomized study. J Natl Cancer Inst 2001;93:1385–91.

39. Inaguma M, Hashimoto K. Porphyrin-like fluorescence in oral cancer: *in vivo* fluorescence spectral characterization of lesions by use of a near-ultraviolet excited autofluorescence diagnosis system and separation of fluorescent extracts by capillary electrophoresis. Cancer 1999;86:2201–11.

40. Chen JK, Katz RV, Krutchkoff DJ. Intraoral squamous cell carcinoma. Epidemiologic patterns in Connecticut from 1935 to 1985. Cancer 1990;66:1288–96.

AACR American Association for Cancer Research

Cancer Prevention Research

Objective Detection and Delineation of Oral Neoplasia Using Autofluorescence Imaging

Darren Roblyer, Cristina Kurachi, Vanda Stepanek, et al.

Cancer Prev Res 2009;2:423-431. Published OnlineFirst April 28, 2009.